Application of Mixture Tuned Matched Filtering on ASTER Data for Hydrothermal Alteration Mapping Related to Porphyry Cu Deposits in Jabal-Barez Ranges, Kerman Copper Belt, Iran

S. J. Yousefi[1], H. Ranjbar[*2], S. Alirezaei[3], S. Dargahi[1]

[1] Department of Geology, Faculty of Sciences, Shahid Bahonar University of Kerman, Kerman, Islamic Republic of Iran
[2] Department of Mining Engineering, Faculty of Engineering, Shahid Bahonar University of Kerman, Kerman, Islamic Republic of Iran
[3] Department of Geology, Faculty of Earth Sciences, Shahid Beheshti University, Tehran, Islamic Republic of Iran

Abstract

The study area is located in Jabal-Barez Ranges, southeastern part of Kerman Copper Belt (KCB), where the porphyry copper mineralization such as Kerver occurs. This article deals with the enhancement of hydrothermal alteration minerals for exploration of porphyry Cu mineralization, and differentiates intense hydrothermal alteration zones from those with low intensity. Shortwave Infrared (SWIR) bands of ASTER data were used for mineral enhancement. The spectra of representative alteration mineral assemblages consisting of sericite + illite, kaolinite + montmorillonite and epidote + chlorite were extracted from SWIR bands of ASTER. The spectra were applied for mineral discrimination using Mixture Tuned Matched Filtering (MTMF) technique. The image processing results were verified using field observation, spectral measurements, thin section and X-ray diffraction studies of the samples. Findings exhibit ASTER capability to discriminate different alteration zones. Findings also significantly show the role of MTMF algorithm as a useful technique for mineral exploration.

Keywords: ASTER; Hydrothermal alteration; Jabal-Barez; Porphyry Cu deposit; MTMF.

Introduction

Many mineral deposits show surficial features such as hydrothermal alterations, gossan, structures, etc. Remote sensing is a standard procedure in mineral exploration which allows recognition of such features with lower cost, less time and effort [1].

Porphyry Cu deposits are associated with extensive hydrothermal alteration, generally zoned from an outer propylitic assemblage, dominated by chlorite, epidote and calcite, into inner argillic (kaolinite, dickite and montmorillonite), phyllic (sericite and illite) and potassic (biotite and k-feldspar) zones [2]. A leached zone, developed over pyrite shell of most porphyry deposits, contains various amounts of hematite, limonite, goethite and jarosite [3]. The alteration

minerals typically display specific absorption features in the shortwave infrared (SWIR) electromagnetic spectrum which indicates the potential for mineral enhancement through remote sensing studies [4].

The Advanced Space-borne Thermal Emission and Reflection Radiometer (ASTER) is a multispectral satellite imaging instrument which has provided suitable opportunities for discrimination of certain hydrothermal alteration minerals and mapping of geological structures [5]. The VNIR and SWIR bands of ASTER show detailed spectral characteristics of Fe oxide/hydroxide and alteration minerals, respectively. The SWIR bands are capable of discriminating hydrothermal mineral assemblages consisting of chlorite + calcite + epidote, kaolinite + montmorillonite, and sericite + illite. The field and the known spectral libraries (such as USGS, JPL and IGCP) exhibit that chlorite; epidote and calcite (propylitic zone) are characterized by a diagnostic absorption feature at 2.35 µm (coinciding with ASTER band 8). Kaolinite, montmorillonite and other clay minerals which are indicators of argillic zone display doublet-shaped intense absorption features near 2.165 and 2.205 µm (corresponding with ASTER bands 5 and 6, respectively). Sericite and illite (phyllic zone) show an intense absorption feature at 2.205 µm which coincides with ASTER band 6.

Many researches display the importance of remote sensing in discriminating alteration minerals using SWIR data through some image processing techniques such as spectral angle mapper (SAM) [6], and principal components analysis (PCA) [7]. These researches highlight hydrothermal alteration minerals on a regional scale through per pixel analysis with little attention to sub pixel analyses. However, a pixel of image is usually derived from the energy which is emitted or reflected from different objects and cannot be highlighted by per pixel classification techniques. There is an extensive literature on discrimination of alteration minerals using sub-pixel technique [8]. These studies used sub-pixel algorithms (such as MF, MTMF, CEM and LSU) to enhance alteration minerals. Alteration mineral abundance may also be applied as an exploration key to highlight alteration zones of mineral prospect with high potential compared to those of low potentials. Mineralization zones of porphyry deposits are compatible with the hydrothermal alteration zones in such a way that the ore zones with a 0.5% copper grade are typically located in the overlapped phyllic and potassic zones. The size and intensity of hydrothermal alteration zones may indicate the intensity of mineralized zones. Also, more studies are required to understand whether it is possible to determine high-potential mineralization zones by applying image processing techniques.

The main purpose of this research is to discriminate and map different types of alteration minerals that associate with porphyry deposits via SWIR bands of ASTER data processing using MTMF technique, and to highlight hydrothermal alteration with low and high intensity in Jabal-Barez Ranges. The initial geological surveys conducted by geological survey of Iran in 2000, and drilling in Kerver deposit by national Iranian Copper Industries Company (NICICo) exhibit the potential for porphyry style mineralization in this area.

Geological setting

Porphyry copper deposits in Iran mainly occur within the Central Iranian Cenozoic Magmatic Belt (CICMB) [9]. They are generally widespread in the southeastern belt segment, the so-called Kerman Copper Belt (KCB) [10] (Fig. 1). The KCB is a narrow linear belt (50-80 km) associated with calc-alkaline extrusive and intrusive rock types [11]. The KCB, generated during the successive stages of Neo-Tethyan ocean closure, consists of subduction in the Cretaceous-Oligocene and continental-continental collision during the late Paleogene-Neogene [12]. The collisional tectonics during the Late Paleogene-Neogene formed a fertile metallogenic setting with significant porphyry systems in the KCB [13].

Cenozoic magmatism and porphyry style mineralization along KCB are characterized by different geological occurrences [14]. In the Middle Eocene, volcanism started to generate Bahr-Aseman complex which includes trachy-andesitic to trachy-basaltic lava flows, tuffs, volcanic breccias and pyroclastic materials. The volcanism continued in the Upper Eocene to make up the Razak volcanic complex which comprises basaltic-rhyolitic and volcano-clastic alternatives [14]. Also, these volcanic complexes are interbedded with marine sedimentary rocks. In the Late Eocene-Oligocene, Bahr-Aseman and Razak volcanic-sedimentary complexes were intruded by the intrusive bodies, some of which are of batholith size. The intrusions are composed of diorite, granodiorite, granite and they locally consist of gabbros [14] and display a high- to medium-K calc-alkaline affinity [14]. These intrusive rocks are identified as the Jabal-Barez granitoids [15], named after the Jabal-Barez mountain ranges in the southern part of KCB where these granitoids extensively exposed. In the Middle Oligocene, volcanic activities formed Hezar volcanic complex which is composed of trachy-basalt and trachy-andesite alternatives that are covered unconformably by limestones and red beds from the Upper Oligocene to the Middle Miocene [15]. Magmatic reactivation
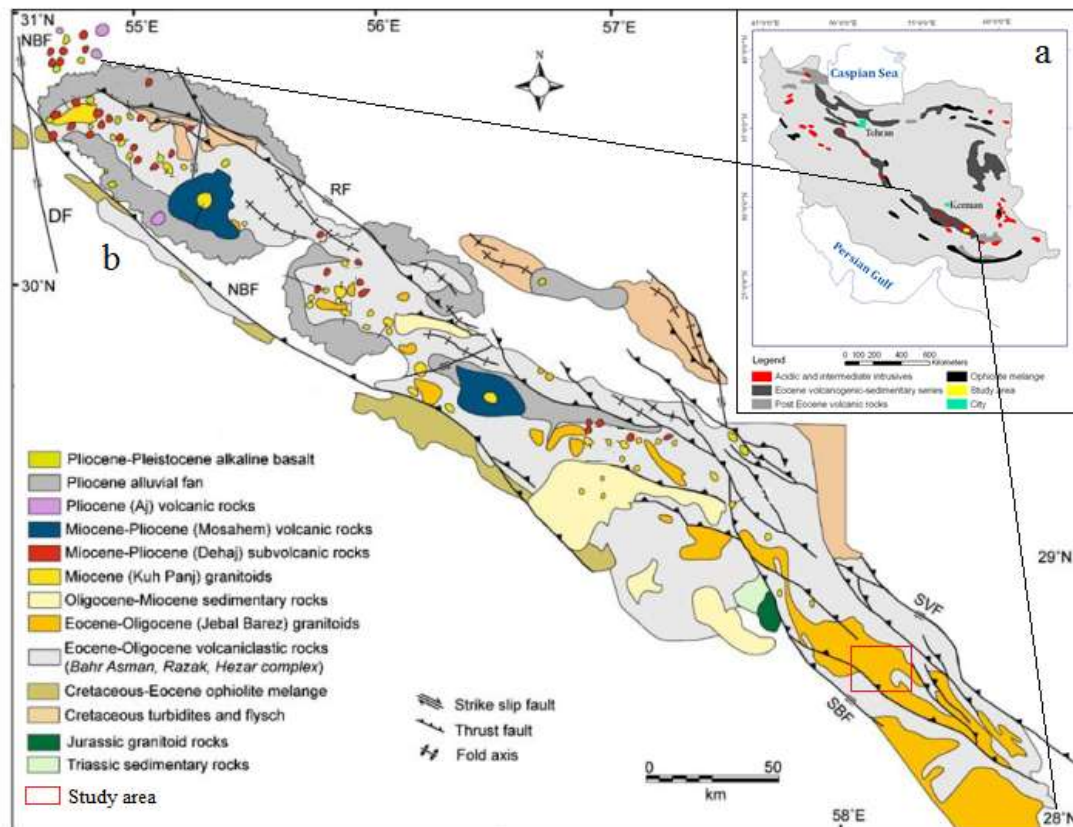
Figure 1. a. Simplified Geological map of major volcanic and plutonic belts of Iran [15], that exhibits the location of Kerman Copper Belt (KCB) in the Urumieh–Dokhtar Volcanic Arc; b. Simplified geological map of the KCB and location of study area [9].

occurred in the Middle and Upper Miocene and numerous shallow intrusions cut the older volcanic and intrusive rocks in KCB [15]. The composition of these intrusive rocks varies from diorite and quartz-diorite to granodiorites with the quartz-diorites dominating rock types [14]. The intrusive bodies are associated with porphyry copper mineralization in KCB and are identified as Kuh-Panj type granitoids, named after the Kuh-Panj mountain in the southeast of Sar Cheshmeh porphyry deposit [15]. These rocks show features of I-type magmas and have a high-K calc-alkaline geochemistry [15]. Moreover, majority of the porphyritic intrusive bodies display high Sr/Y and La/Yb ratios, which exhibit adakitic affinity [16]. The youngest volcanism features in the KCB are of Late Miocene-Pliocene age and include dacitic domes, olivine-alkali basalts, foidites, lamprophyres and volcanic edifies such as the Masahim stratovolcano [17].

The Jabal-Barez granitoid batholith is the major geological unit in Jabal-Barez Ranges (Fig. 2) that intruded the Eocene volcano-sedimentary rocks and is extensively exposed and covers an area of about 750 km^2. According to previous studies such as [15], the

Jabal-Barez batholith is related to the Late Eocene-Oligocene. This granitic batholith was subsequently intruded by intrusive bodies such as Kerver. These intrusions may be associated with porphyry style mineralization and are similar to the other intrusions in KCB that generated porphyry copper deposits such as that of Sar Cheshmeh. The Eocene volcano-sedimentary rocks are not important in Jabal-Barez area and are poorly exposed. This is mainly observed in the margin of Jabal-Barez granitic batholith (Fig. 2).

Materials and Methods

ASTER images with L1B preprocessing level, acquired on 06/09/2001, were used in this study. ASTER data pre-processing procedure was applied for cross-talk, geometric and atmospheric corrections. Cross-talk correction procedure was used on the SWIR data to omit the effects of energy dispersion from band 4 into bands 5 and 9 [18]. The VINR and SWIR bands were then stacked into one dataset so that all bands acquired the same spatial resolution (15 m). The Internal Average Relative Reflectance (IARR)
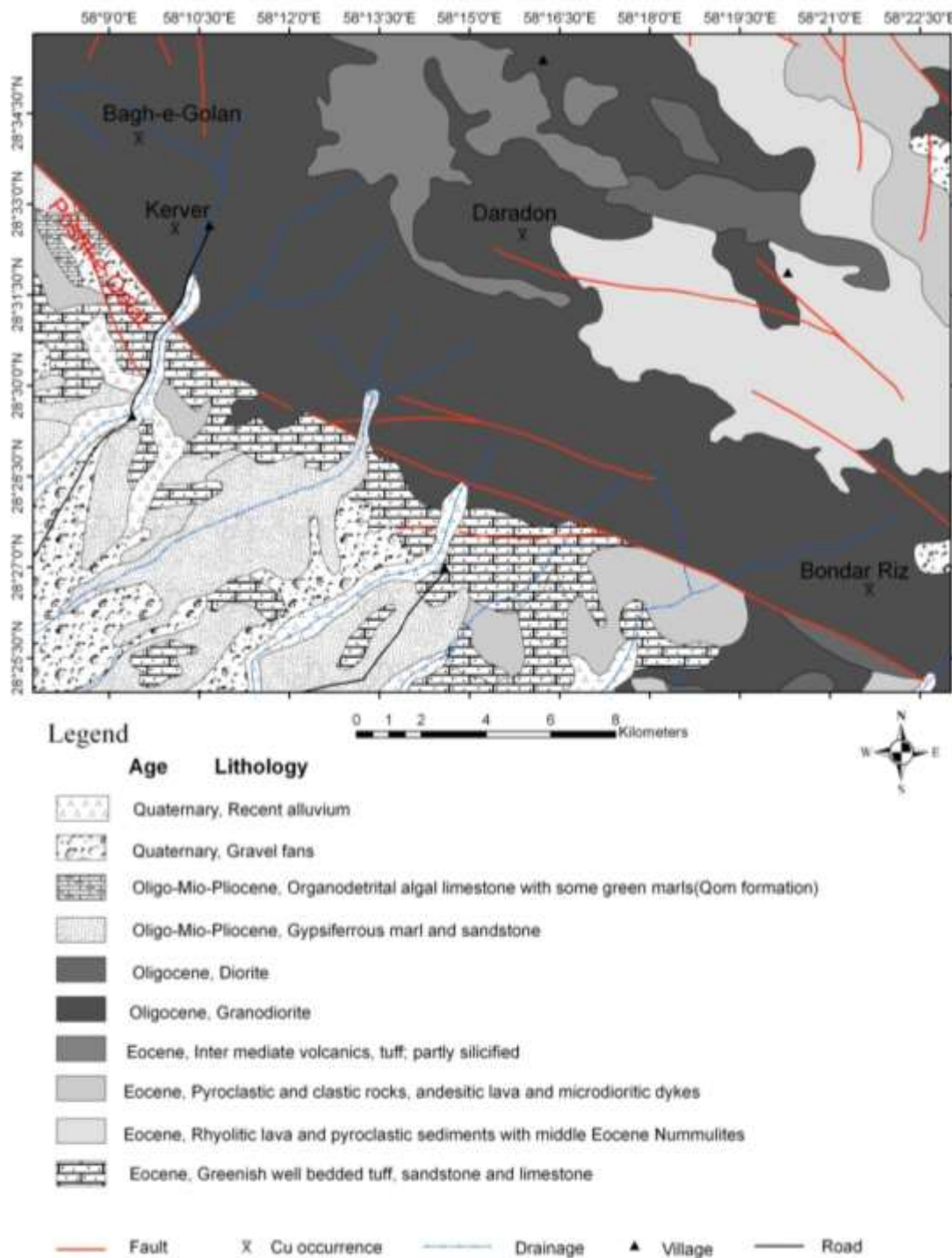
273

Figure 2. Geological map for the Jabal-Barez ranges, modified after [24]

calibration technique was applied for radiometric correction. The IARR is a satisfactory technique for the arid and semiarid areas where the vegetation cover is poor. In this technique, an average spectrum is calculated by using the satellite image and is applied as

a reference spectrum [19]. The pixels in each image are then divided by the mean value of the entire scene [20]. The imagery that was geo-referenced to a UTM Zone 40 north projection with WGS-84 datum was once more ortho-rectified and reprojected by using ground control

points which were selected from topographic data with a scale of 1:25000 and a total RMS error of 2.9 meters.

3.1. End member extraction

The different hydrothermal alteration types were sampled in the 34-day geological field survey and the spectra of hydrothermally altered samples were measured using a fieldSpec[3®]spectroradiometer (Analytical Spectral Devices, Inc., Boulder, CO, USA in the Technical University of Kerman in Mahan, Iran). The spectrometry results were used to study the spectral characteristics of different hydrothermal alteration types. The spectral measurement results were compared with the USGS spectral library and the results of the X-ray diffraction (XRD) analyses. Based on the results of the acquired XRD and spectrometry analyses of altered samples, different hydrothermal alteration types were investigated through a geological survey and thin section studies. The reference spectra of different alteration minerals were extracted from ASTER data using a z-profile method.

3.2. Image processing

MTMF is an advanced type of spectral mixture analysis and is based on a signal processing procedure that is used for sub-pixel mapping of target alteration minerals [21]. This technique utilizes the spectra of end members extracted from imageries or chosen from a spectral library. MTMF algorithm includes two phases: 1. a matched filter (MF) calculation for abundance estimation, 2. a mixture tuning calculation for the identification and rejection of false positives [22]. The spatial power in the MTMF procedure is in the mixture tuning that calculates a value of infeasibility for every matched filter classified pixel [22] that maps the mineral target abundance in the presence of unknown spectrum of mixed background. The computation of minimum noise fraction (MNF) for the input imageries is necessary for this image processing technique. MNF method reduces the dimension of data via the transformation of a standard principal component, and also distinguishes the noise via the estimation of the covariance matrix. In this technique, the pure pixels that are the same as the target mineral spectra are identified in the first step. Then, the pure pixels without close matching with the target mineral spectra are characterized as infeasibility values and are applied for identification of background spectrum. Therefore, the values of background and target spectra are identified. The findings of MTMF technique are accessible as MF and infeasibility. Investigation of the results obtained from these two images in a two dimensional space makes it possible to choose the pixels with low infeasibility and high MF [22].

Results and Discussion

Based on the field and laboratory observations and mineralogical studies, secondary biotite + K-feldspar (potassic alteration), sericite + quartz (phyllic), kaolinite + montmorillonite (argillic) and epidote (epidptization) are the major alteration minerals' assemblages in the study area (Fig. 3). Iron oxide/hydroxide also stained the phyllic and argillic alterations (Fig. 3c). The spectral characteristics of the alteration minerals were specified in the study area, and their spectral bands in the ASTER data are shown in Table 1.

A comparison between laboratory spectra and USGS spectral library is shown in Fig. 4. Muscovite/illite display a prominent Al-O-H spectral absorption feature typically at 2.20 µm (6th ASTER band), and a less prominent absorption shoulder at 2.33 µm (Aster band 8), due to Mg- Fe-O-H absorption. Moreover, phyllic alteration is stained by iron oxide/hydroxide. Muscovite and illite laboratory spectra show a spectral absorption feature near 0.44 µm due to iron oxide/hydroxide

Table 1. Spectral characteristics of alteration minerals reported from field observations, mineralogical studies and XRD analysis, and their features in VNIR-SWIR bands of ASTER

Alteration minerals	Absorption feature (µm)	Resampled to VNIR-SWIR bands
Muscovite/illite	2.2 and minor absorption in 2.32	Band 6 and 8
Kaolinite/montmorillonite	2.17 and 2.20	Band 5 and 6
epidote	2.32	band 8

Table 2. A comparison between size of mineral occurrences and intensity of hydrothermal alterations

| Mineral occurrences	Mineral occurrence size	Phyllic	Argillic
Kerver	1.6 km^2	Moderate alteration weakly developed	Moderate alteration weakly developed
Bagh Golan	1.8 km^2	Intense alteration weakly developed	Moderate alteration weakly developed
Daradon	5 km^2	Intense alteration	weak
Bondar-Riz	9 km^2	Intense alteration	Intense alteration
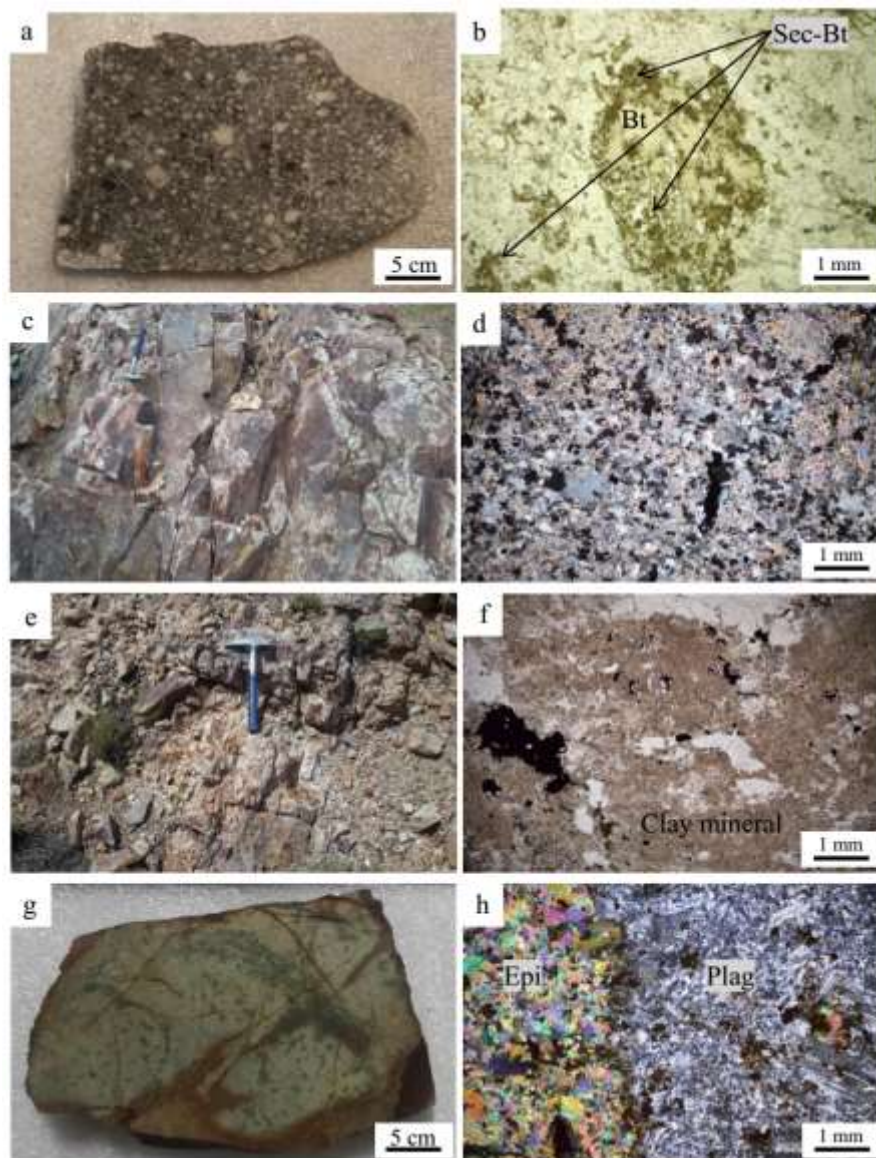
Figure 3. Close-up view of outcrop, hand-specimens and Photomicrograph displaying the occurrence of hydrothermal alteration at the study area; a. Slab of porphyry intrusion with potassic alteration, b. Photomicrograph of a potassic alteration from Slab shown in (a) that secondary biotite formed in margin of magmatic biotite, also secondary biotite dispersed in the groundmassc. Close-up view of phyllic outcrop that stained by iron oxide/hydroxide, d. Photomicrograph of a phyllic alteration collected from outcrop shown in (c). Sericite and quartz are the major mineral phases, e and f. Close-up view of outcrop and photomicrograph of argillic alteration. Clay minerals in photomicrograph have brown color, g and h. Slab and photomicrograph of epidotization that epidote is a major mineral phase in the rocks. (Bt: Biotite; Sec-Bt: Secondary Biotite; Plag: Plagioclase; Epi: Epidote)

staining. Kaolinite/ montmorillonite developed in argillic alteration zone are characterized by doublet absorption features at 2.20 µm (6th ASTER band) and 2.17 µm (5th ASTER band), respectively. Epidote, the major mineral in epidotized rocks, displays an intense absorption feature at 2.33µm (8th ASTER band) due to CO_3 and Fe- Mg-O-H vibrational bonds. Moreover, the muscovite/illite, kaolinite/montmorillonite and epidote display intense reflection in 4th ASTER band.

Spectra of field samples and USGS spectral library are resampled from visible to shortwave infrared bands (VNIR-SWIR) of ASTER data to compare the bands with the spectra derived from image by z-profile technique for muscovite/illite, kaolinite/ montmorillonite, and epidote (Fig. 4). The image derived spectra display absorption features in band 6 for muscovite/illite, in the 5th and 6th bands of ASTER for kaolinite/montmorillonite and in band 8 for epidote.
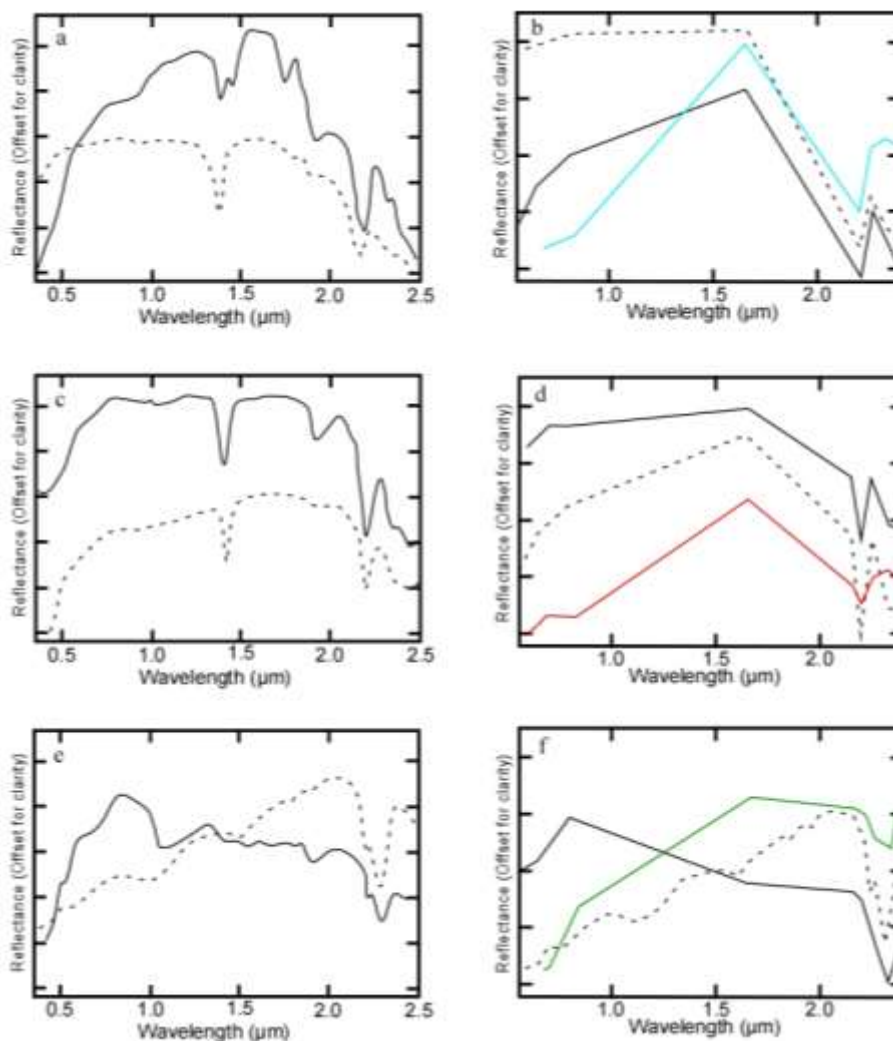
Figure 4. a. USGS spectra (dashed lines) and laboratory spectra (solid lines) at full resolutions (420 bands)of kaolinite/montmorillonite that show Al–OH absorption features at 2.20, b. USGS spectra (dashed lines) and laboratoryspectra (black solid lines)re-sampled to the 9 VNIR + SWIR bands of ASTER data, and spectra extracted from the imageries for kaolinite/montmorillonite (turquoise solid line) showing Al–OH absorption features at 2.20, c. USGS spectra (dashed lines) and laboratoryspectra (solid lines) at full resolutions (420 bands)of muscovite/illite that display Al–OH absorption features at 2.20, d. USGS spectra (dashed lines) and laboratoryspectra (black solid lines)re-sampled to the 9 VNIR + SWIR bands of ASTER data, and Spectra extracted from the imageries for muscovite/illite (red solid line) showing Al–OH absorption features at 2.20, e. USGS spectra (dashed lines) and laboratory spectra (solid lines) at full resolutions (420 bands) of epidote that exhibit Mg–OH absorption features at 2.31–2.33 μm, f. USGS spectra (dashed lines) and laboratory spectra (black solid lines) re-sampled to the 9 VNIR + SWIR bands of ASTER data, and spectra extracted from the imageries for epidote (green solid line) showing Mg–OH absorption features at 2.31–2.33 μm.

Also, an absorption feature in the 1st band of ASTER data can be related to iron oxide/hydroxides that stained altered rocks. The comparison shows that spectral characteristics of alteration minerals can be extracted from imageries, and these spectra may be used as end members for further image processing.

Sub-pixel analysis of visible through shortwave infrared bands allowed semi-quantitative analyses of hydrothermal alteration minerals. Furthermore, the

infeasibility and MF score bands were used to produce a 2-dimensional scatter plot for selecting pixels with low infeasiblity and higher MF score. For mineral fractions at each pixel and creating a mineral classification map, pixels of low infeasibility and MF scores more than 0.6 were selected and classified into three groups. These values exhibited the percentages of each alteration minerals. For example, 0.60 indicates that 60 percent of pixel included the chosen mineral. The areas

accommodated with those pixels were draped over the 4th band of ASTER gray scale imagery (Figs. 5 and 6). The highlighted areas are in agreement with the hydrothermal alterations around the mineral occurrences

such as Kerver, Daradon, Bondar-Riz, and Bagh Golan.

Investigation of highlighted alteration minerals exhibited that mineral assemblage of propylitic alteration has not well developed around the mineral
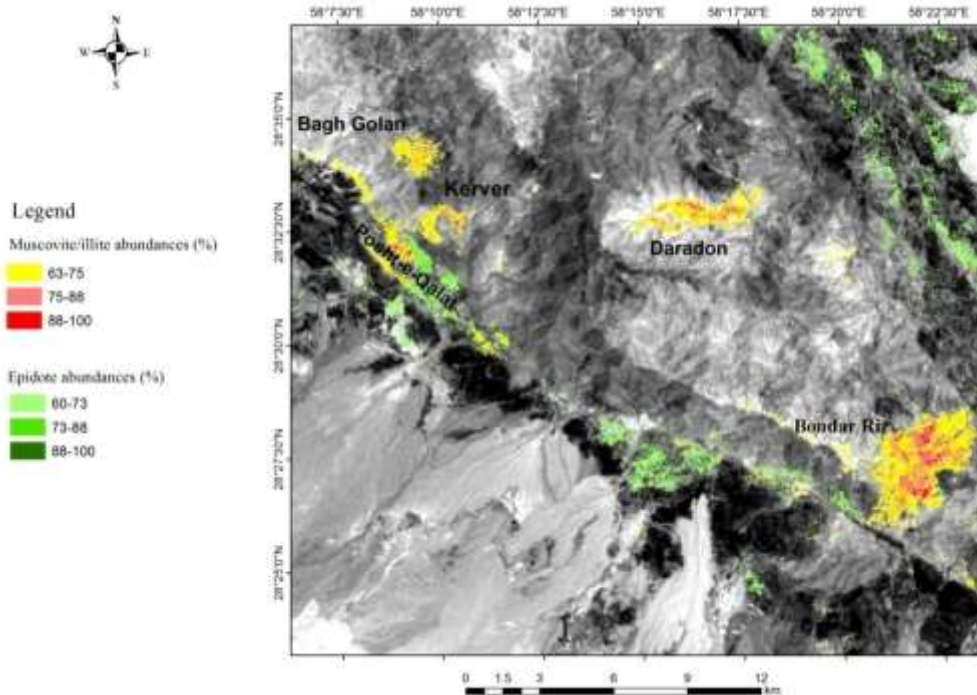

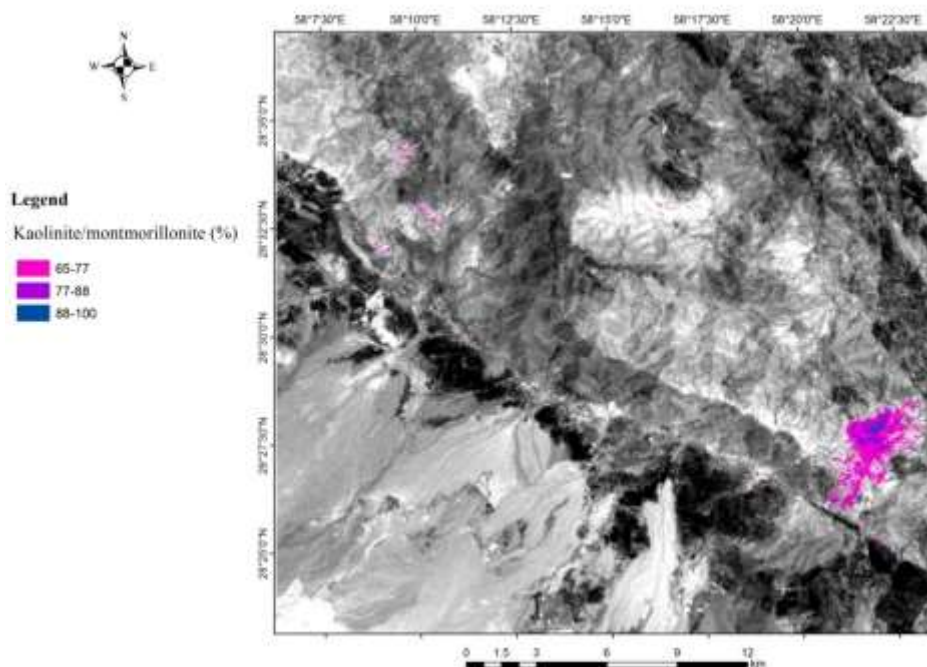**Figure 5.** Spatial distribution of muscovite/illite and epidote abundances, derived from the MTMF technique.

Figure 6. Spatial distribution of kaolinite/montmorillonite abundances derived from the MTMF technique.

278

occurrences. This feature may be due to the low abundance of Fe- Mg- oxides in the host rocks (Jabal-Barez granitic batholith). However, epidote is highlighted along the Jabal-Barez fault in Eocene volcano-sedimentary rocks in the margin of Jabal-Barez batholith. Muscovite/illite is the major alteration mineral that exposed in the study area. The highlighted alteration minerals in the mineralized zones such as Kerver, Daradon, Bondar-Riz and Bagh Golan displayed elliptical to circular shape with muscovite/illite as dominant alteration minerals and sporadic kaolinite/montmorillonite (Figs. 5 and 6).

The MTMF findings define an estimation of mineral sub-pixel fractions demonstrating the abundance of alteration minerals at each pixel. In Table 2, four mineral occurrences were considered to understand whether the fractions correspond to the size and intensity of alteration minerals. The high fraction values (88-100) of muscovite/illite, and kaolinite/montmorillonite were considerably distinguished at Bondar-Riz mineral occurrence. While, the Daradon occurrence shows moderate to high fraction values (75-100) of muscovite/illite without considerable argillic alteration. Also, Kerver and Bagh Golan mineral occurrences exhibit low to moderate fraction of muscovite/illite (63-88) with negligibly low fraction of argillic alteration. These results show that the areas with intense hydrothermal alterations are bigger than those with low intensity hydrothermal alterations.

Data validation

The alteration minerals highlighted by MTMF technique were assessed in the field and laboratory. The fieldworks were carried out in the four hydrothermally altered areas, and 256 samples were collected through unaltered, hydrothermally altered, mineralized and gossan zones of Kerver, Daradon, Bondar-Riz and Bagh Golan mineral occurrences. Microscopic studies, X-ray diffraction and spectral analyses were carried out on the samples. Then, the veracity of alteration minerals enhancement was considered by carrying out a visual assessment in which the accuracy of determined alteration minerals was checked while taking into account the corresponding collected samples that were investigated by mineralogical and spectral features. The field assessment of highlighted alteration minerals exhibits a good correlation with ASTER alteration map (Figs. 5 and 6).

Also, to assess the accuracy of the produced alteration maps, random samples were collected and studied in the laboratory for the minerals' content. These alteration minerals so obtained were compared with the highlighted alteration minerals using ASTER data. A confusion matrix was prepared and the map accuracy was determined. The calculated accuracies for muscovite/illite, kaolinite/montmorillonite, and epidote were 84%, 76% and 65%, respectively. These results exhibit those alteration minerals which represent the hydrothermal alteration types mapped with an accepted level of accuracy.

Conclusion

The application of MTMF technique on ASTER data for mapping the regional development of alteration minerals in Jabal-Barez ranges of Kerman copper belt in Iran is helpful in mapping and enhancing hydrothermal alterations related to porphyry type mineralization. Field observations, sampling and mineralogical analyses were carried out to validate the inferred hydrothermal alteration zones based on image processing. The findings display the presence of intense phyllic and argillic alteration types around many mineral occurrences. Unlike other porphyry type deposits, this area does not show a well-developed propylitic alteration. The fieldworks and petrography of host rocks exhibit that Jabal-Barez granitic batholith hosted the porphyry mineral occurrences in Jabal-Barez Ranges. Thus, the absence of propylitic alteration around the porphyry mineral occurrence may be due to the low abundance of Fe- Mg- oxides in the granitic host rocks.

While combined with fieldworks, the application of ASTER data supplies useful data to determine areas that are more appropriate for Cu mineralization. Also, the results exhibit that spectral unmixing is precise for mineral exploration. Comparisons of sub-pixel abundance maps with the known mineral occurrences displayed a reasonable conformity. Therefore, areas with higher fractions of hydrothermal alteration are in agreement with important mineral occurrences.

References

1. Abrams M., Tsu H., Hulley G., Iwao K., Pieri D., Cudahy T. and Kargel J. The Advanced Spaceborne Thermal Emission and Reflection Radiometer (ASTER) after fifteen years: Review of global products. *Int. J. Appl. Earth Obs.*, **38**: 292-301 (2015).
2. Aramesh Asl R., Afzal P., Adib A. and Yasrebi A.B.

Application of multifractal modeling for the identification of alteration zones and major faults based on ETM+multispectral data. *Arab. J. Geosci.,* **8**(5): 2997-3006 (2015).

3. Tommaso I.D. and Rubinstein N. Hydrothermal alteration mapping using ASTER data in the Infiernillo porphyry deposit, Argentina. *Ore Geol. Rev*., **32**(2): 275-290 (2007).

4. Crosta A.P., DE Souza Filho C.R., Azevedo F. and Brodie C. Targeting key alteration minerals in epithermal deposit in Patagonia, Argentina, using ASTER imagery and principal component analysis. *Int. J. Remote Sens*, **10**(21): 4233-4240 (2003).

5. Amer R., Mezayen A. and Hasanein M. ASTER spectral analysis for alteration minerals associated with gold mineralization. *Ore Geol. Rev.,* **75**: 239-251 (2016).

6. Tangestani M.H., Mazhari N., Agar B. and Moore F. Evaluating Advanced Spaceborne Thermal Emission and Reflection Radiometer (ASTER) data for alteration zone enhancement in a semi-arid area, northern Shahr-e-Babak, SE Iran. *Int. J. Remote Sens.,* **29**(10): 2833-2850 (2008).

7. Tangestani M.H. and Moore F. Comparison of three principal component analysis techniques to porphyry copper alteration mapping a case study in Meiduk area, Kerman, Iran. *Can. J. Remote Sens.,* **27**(2): 176–182 (2001).

8. Maroufi K., Hezarkhani A. and Asadzadeh S. Mapping the alteration footprint and structural control of Taknar IOCG deposit in east of Iran, using ASTER satellite data. *Int. J. Appl. Earth Obs*., **33**: 57-66 (2014).

9. Shafiei B., Haschke M. and Shahabpour J. Recycling of OrogenicArc Crust Triggers Porphyry Cu Mineralization in Kerman Cenozoic Arc Rocks, Southeastern Iran. *Miner Deposita* **44**: 265–283 (2009).

10. Yousefi S.J., Ranjbar H., Alirezaei S., Dargahi S. and Lentz D.R. Comparison of hydrothermal alteration patterns associated with porphyry Cu deposits hosted by granitoids and intermediate-mafic volcanic rocks, Kerman Magmatic Arc, Iran: Application of geological, mineralogical and remote sensing data. *J Afr Earth Sci*, **146**: 112-123 (2018).

11. Mars J.C. Regional Mapping of Hydrothermally Altered Igneous Rocks Along the Urumieh–Dokhtar, Chagai, and Alborz Belts of Western Asia Using Advanced Spaceborne Thermal Emission and Reflection Radiometer (ASTER) Data and Interactive Data Language (IDL) Logical Operators — A Tool for Porphyry Copper Exploration and Assessment. U.S. Geological Survey. *Sci. Inv. Rep.,* **2010–5090-O**: 36 (2014).

12. Moradi M., Basiri S., Kananian A. and Kabiri K. Fuzzy logic modeling for hydrothermal gold mineralization mapping using geochemical, geological, ASTER imageries and other geo-data, a case study in Central Alborz, Iran. *Earth Sci. Inform.,* **8**: 197-205 (2015).

13. Zarasvandi A., Liaghat S. and Zentilli M. Geology of the Darreh-Zerreshk and Ali-Abad porphyry copper deposits, Central Iran. *Int. Geol. Rev*., **47**(6): 620-646 (2005).

14. McInnes B.I.A., Evans N.J., Belousova E. and Griffin W.L. Porphyry Copper Deposits of the Kerman Belt, Iran: Timing of Mineralization and Exhumation Processes. *CSIRO Scientific Research Report*, **41** (2003).

15. Yousefi S.J., Ranjbar H., Alirezaei S. and Dargahi S. Discrimination of Sericite Phyllic and Quartz-rich Phyllic Alterations by Using a Combination of ASTER TIR and SWIR Data to explore Porphyry Cu Deposits Hosted by Granitoids, Kerman Copper Belt, Iran. *J. Indian Soc. Remote Sens.*, doi.org/10.1007/s12524-017-0745-z.

16. Richards J.P., Spell T., Rameh E., Razique A. and Fletcher T. High Sr/Y Magmas Reflect Arc Maturity, High Magmatic Water Content, and Porphyry Cu $\pm$ Mo $\pm$ Au Potential: Examples from the Tethyan Arcs of Central and Eastern Iran and Western Pakistan. *Econ. Geol.,* **107**: 295–332 (2012).

17. Atapour H. Geochemistry and Metallogenic of Igneous Rocks in Dehaj–Sardoieh Belt, Kerman, Iran. Ph.D. Thesis, Shahid Bahonar University of Kerman, Kerman: 280 (2007).

18. Tayebi M., Tangestani M., Vincent R. and Neal D. Spectral properties and ASTER-based alteration mapping of Masahim volcano facies, SE Iran. *J. Volcanol. Geoth. Res.,* **287**: 40-50 (2014).

19. Zoheir B. and Emam A. Field and ASTER imagery data for the setting of gold mineralization in Western Allaqi–Heiani belt, Egypt: A case study from the Haimur deposit. *J. Afr. Earth Sci.,* **99**(1): 150-164 (2014).

20. Son Moon Y.S., Kang K. and Yoon W.J. Lithological and mineralogical survey of the Oyu Tolgoi region, Southeastern Gobi, Mongolia using ASTER reflectance and emissivity data. *Int. J. Appl. Earth Obs.,* **26**: 205-216 (2014).

21. Laeiq A., Tahir S. and Khan S.D. Reflectance spectroscopy and remote sensing data for finding sulfide-bearing alteration zones and mapping geology in Gilgit-Baltistan, Pakistan. *Earth Sci. Inform.,* **9**(1): 113-121 (2016).

22. Mundt J.T., Streutker D.R. and Glenn N.F. Partial Unmixing of Hyperspectral Imagery: Theory and methods. *ASPRS Annual Conference Tampa, Florida*, 1-12 (2007).

23. Eldosouky A.M., Abdelkareem M. and Elkhateeb S. Integration of remote sensing and aeromagnetic data for mapping structural features and hydrothermal alteration zones in Wadi Allaqi area, South Eastern Desert of Egypt. *J. Afr. Earth Sci.,* **130**: 28-37 (2017).

24. Valeh N., Pazirandeh M., Tehrani K. and Mitrovie R. Geological map of Jabal-Barez, (1:100000), *Geological survey of Iran*: Sheet 7647 (1973).